smooth decay in Fig. 8, some structure can be seen in the x-ray flux.

We feel that the stabilizing effect of hot electrons should not be overlooked in the planning of thermonuclear experiments.

Note added in proof. A lower limit to the heating efficiency of the electron beam is easily calculated, and is found to be surprisingly high. The heating efficiency is defined as the ratio of the steady-state loss of power from the plasma to the input power of the beam. A lower limit to the power loss from the plasma is given by the total energy stored in the plasma divided by its decay time constant. Any instability during steady-state operation would cause the plasma to be lost faster, and give a larger value to the power loss. An upper limit to the power input is the power drain on the power supply. Since some of the electron beam does not pass through the hollow anode and does not reach the plasma, this number is too big. The largest ratio of these two numbers is found in the short-lifetime experiments using the diamagnetic loop. Here the lower limit to the heating efficiency is about one percent.

ACKNOWLEDGMENTS

We wish to thank our associates in the Thermonuclear Division for their criticism and encouragement, the laboratory administration for its support, and J. G. Harris whose technical skill made these experiments possible.

PHYSICAL REVIEW VOLUME 136, NUMBER 3A 2 NOVEMBER 1964

Magnetic Properties of the Canted Antiferromagnet α-$CoSO_4$†

I. F. SILVERA, J. H. M. THORNLEY,* AND M. TINKHAM
Department of Physics, University of California, Berkeley, California
(Received 27 May 1964)

It is known from neutron scattering experiments that α-$CoSO_4$ is a four-sublattice canted antiferromagnet with no net magnetic moment. In this paper the magnetic properties of this material are analyzed using a model in which an isotropic fictitious spin of $\frac{1}{2}$ is assigned to each Co^{++} ion. The large canting angle of 25° is interpreted in terms of antisymmetric terms in the Hamiltonian due to anisotropic superexchange and the large anisotropy in the g values. Corresponding to the four sublattices, there are four spin-wave modes at $k=0$. Calculations indicate that the resonant frequencies of these modes should lie in the far infrared, and that only three of the modes should be observable spectroscopically. In addition, static susceptibilities of the system have been calculated for $T=0$ and $T\gg T_N$ (12°K), and the g values have been estimated. Far-infrared transmission experiments have resulted in the observation of three lines at 20.6, 25.4, and 35.8 cm^{-1}, with relative intensities 1:1:0.1. Although these lines are presumed to be the three expected resonances, an unambiguous fitting for all the parameters of the model has not been possible. The temperature dependence of the resonance lines is anomalous.

I. INTRODUCTION

FOR several years there has been much interest in canted magnetic systems. Purely on grounds of symmetry and the thermodynamics of phase transitions, Dzialoshinski[1] first suggested the form of the interaction which gives rise to the canting. Moriya[2] included the effect of spin-orbit coupling in the superexchange Hamiltonian of a system with a nondegenerate orbital ground state to find, in addition to the usual isotropic exchange and the well-known symmetric anisotropic exchange (which finds its origin in the combined effects of the spin-orbit coupling and the crystal field), that there is a further exchange term which is antisymmetric with respect to the interacting spins $\mathbf{S}_i$ and $\mathbf{S}_j$ and is of the form

$$\mathcal{H}_m=\mathbf{D}_{ij}\cdot\mathbf{S}_i\times\mathbf{S}_j. \quad (1)$$

Here $\mathbf{D}_{ij}$ is a vector that depends linearly on the spin-orbit coupling constant, the precise form being derived in Moriya's paper. In most of the canted antiferromagnetic crystals which have been investigated, for example, α-Fe_2O_3,[1] $MnCO_3$,[3] $KMnF_3$,[4] and $CuCl_2\cdot 2H_2O$,[2] the canting angle has been found to be of the order of 1°.

α-$CoSO_4$ has an orthorhombic crystal structure and a four-sublattice canted antiferromagnetic structure having zero net magnetic moment. Its magnetic structure was first determined in the neutron diffraction experiment of Frazer and Brown.[5] They, however, were not at the time of their first paper, aware of the existence of the two forms of $CoSO_4$ (see Sec. III), as they attempted to explain the static susceptibility measure-

† Supported in part by the U. S. Office of Naval Research, The National Science Foundation, and the Alfred P. Sloan Foundation.
* Present address: Clarendon Laboratory, Oxford, England.
[1] I. Dzialoshinski, Phys. Chem. Solids 4, 241 (1958).
[2] T. Moriya, Phys. Rev. 120, 91 (1960).
[3] A. S. Borovik-Romanov, Zh. Eksperim. i Teor. Fiz. 36, 539 (1959) [English transl.: Soviet Phys.—JETP 9, 539 (1959)].
[4] A. J. Heeger, Olaf Beckman, and A. M. Portis, Phys. Rev. 123, 1652 (1961).
[5] B. C. Frazer and P. J. Brown, Phys. Rev. 125, 1283 (1962); P. J. Brown and B. C. Frazer, *ibid.* 129, 1145 (1963).

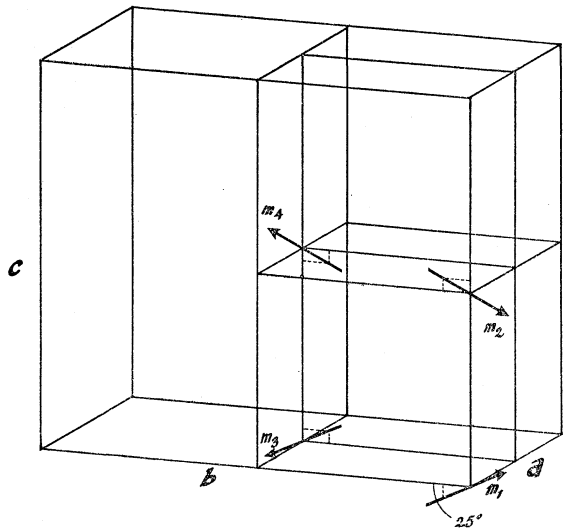

FIG. 1. The magnetic structure of α-$CoSO_4$ as determined by neutron diffraction measurements. The magnetic moments are coplanar and canted within the bc plane ($\mathbf{m}_1=-\mathbf{m}_3$, $\mathbf{m}_2=-\mathbf{m}_4$).

ments of Borovik-Romanov and Kreines[6] on what is now known[5] to be β-$CoSO_4$ in terms of the magnetic structure they had found for α-$CoSO_4$. The neutron diffraction measurements showed that the magnetic unit cell and the chemical unit cell are identical and that the magnetic moments are aligned as shown in Fig. 1. The four magnetic moments are coplanar and lie in the bc plane, inclined to the b axis at a canting angle of 25°. The magnitude of the moment was found to be 3.3 ± 0.2 Bohr magnetons at 4.2°K. The magnetic moments and their environments are identical except for orientation, and can be brought into one another by the symmetry operations of the crystal.

In this paper we present the far-infrared magnetic spectrum of α-$CoSO_4$ which resulted from low-temperature transmission experiments on pressed powder samples.[7] Three antiferromagnetic resonance lines were observed. This is the number allowed for a coplanar four-sublattice model, as has been shown by Joenk for $CuCl_2\cdot 2H_2O$.[8] A further purpose of this paper is to attempt to correlate the various low-temperature properties of α-$CoSO_4$ with each other, using a molecular field model. Uryu[9] has also attacked this problem, but using rather different techniques. In a spin Hamiltonian in which he has omitted the important exchange interactions between Co_1 and Co_4 or Co_2 and Co_3 (see Figs. 1 and 4), he replaces the spin operators by classical spin vectors. He derives the anisotropy for the magnetic system by a perturbation scheme in which the splittings due to the rhombic distortions from cubic symmetry are considered to be greater than that due to the spin-orbit coupling. His attempt to fit the theory on α-$CoSO_4$ with data available on β-$CoSO_4$ was unsuccessful.

In Sec. II a detailed account of the crystal structure and exchange paths is given, as a good understanding of this is necessary before one can try to comprehend the magnetic behavior of the system; in Sec. III a two-sublattice model of a cobalt salt with a fictitious spin of $\frac{1}{2}$ is considered in order to demonstrate how, symmetry permitting, large canting angles can be obtained with an isotropic exchange Hamiltonian and an anisotropic g tensor; in Sec. IV we show that the exchange Hamiltonian must be anisotropic in both the symmetric and antisymmetric parts and we write down the most general Hamiltonian which is consistent with the crystal symmetry. Section V is devoted to calculating the resonant frequencies, and Sec. VI to the calculation of the rf and the static susceptibilities. In Sec. VII we calculate the Néel temperature and consider the stability of the given magnetic structure; in Sec. VIII we calculate the static susceptibility above the Néel temperature on the molecular field model; in Sec. IX we make a crystal-field calculation in terms of a simple point-charge model to find the g values. Finally, the experimental apparatus and data are discussed in Sec. X and the fitting procedure in Sec. XI.

II. CRYSTAL STRUCTURE

Two forms of $CoSO_4$ are known to exist: α-$CoSO_4$ is the low-temperature modification, stable below about 600°C; above this temperature β-$CoSO_4$ is the stable form. At room temperature β-$CoSO_4$ slowly transforms into α-$CoSO_4$. α-$CoSO_4$ has[10] the space group D_{2h}^{17} and is isostructural with $NiSO_4$,[11] $CrVO_4$,[5] $MgSO_4$,[12] and

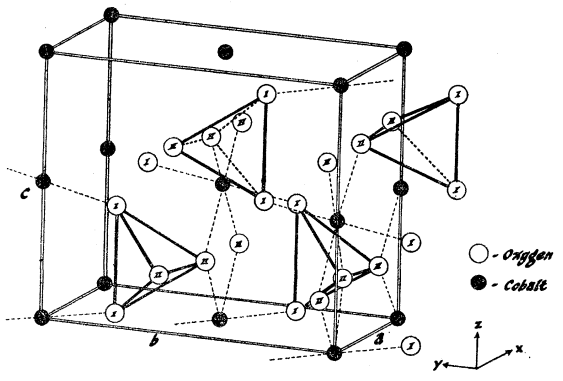

FIG. 2. The chemical cell of α-$CoSO_4$ as determined by x-ray diffraction. For clarity some of the SO_4 tetrahedra and all of the sulfur atoms which are located within the tetrahedra have been omitted. Note that the adjacent oxygen octahedra along the c axis are tilted with respect to one another.

[6] A. S. Borovik-Romanov and N. M. Kreines, Zh. Eksperim. i Teor. Fiz. 35, 1053 (1958) [English transl.: Soviet Phys.—JETP 8, 734 (1959)].

[7] I. F. Silvera and M. Tinkham, Bull. Am. Phys. Soc. 9, 625 (1962); I. F. Silvera, *ibid.* 8, 601 (1963).

[8] R. J. Joenk, Phys. Rev. 126, 565 (1962).

[9] N. Uryu, J. Phys. Soc. Japan 18, 1641 (1963).

[10] P. J. Rentzeperis, Neues Jahrb. Mineral., Monatsch. 10, 226 (1958). Interchange α and β to correspond to present notation.

[11] P. I. Dimaras, Acta Cryst. 10, 313 (1957).

[12] P. J. Rentzeperis and C. T. Soldatos, Acta Cryst. 11, 686 (1958).

$MnSO_4$[13]; β-$CoSO_4$[10] has the space group D_{2h}^{16} and is isostructural with $CuSO_4$ and $ZnSO_4$.[13,14] Methods of preparation are described in the references cited and also by Brown and Frazer[5] and Kreines.[15,16] These will not be detailed here.

The positions of the orthorhombic space group D_{2h}^{17} occupied by the atoms of α-$CoSO_4$ (notation of the International Tables[17]) are as follows:

4 Co in 4 (a); $(0,0,0)$; $(0,0,\frac{1}{2})$,
4 S in 4 (c); $(0,y,\frac{1}{4})$; $(0,-y,\frac{3}{4})$,
8 O_I in 8 (f); $(0,y,z)$; $(0,-y,-z)$; $(0,y,\frac{1}{2}-z)$; $(0,-y,\frac{1}{2}+z)$,
8 O_{II} in 8 (g); $(x,y,\frac{1}{4})$; $(-x,y,\frac{1}{4})$; $(x,-y,\frac{3}{4})$; $(-x,-y,\frac{3}{4})$.

The remaining positions are obtained by adding $(\frac{1}{2},\frac{1}{2},0)$ to those listed above. Rentzeperis[10] has made the most complete analysis of α-$CoSO_4$ and we shall use his results. The lattice constants are

$$a_0=5.200\text{ Å},\quad b_0=7.876\text{ Å},\quad c_0=6.531\text{ Å},$$

and the various parameters are given in Table I. In Fig. 2 we show the chemical cell.

Let us consider the environment of the Co^{2+} ion at (0,0,0) which is surrounded by a distorted oxygen octahedron. Its six nearest neighbors are 2 O_I's at $\pm(0,y,z)$ and 4 O_{II}'s at $\pm(-x+\frac{1}{2},y-\frac{1}{2},\frac{1}{4})$ and $\pm(x-\frac{1}{2},y-\frac{1}{2},\frac{1}{4})$. We note that this environment has inversion symmetry. Figure 3 shows the projections of the 7 ions on the *ab* and *ac* planes. The Co−O and the S−O distances are also relevant and we list them in Table II.[10]

Finally, the O_I-O_I, O_I-O_{II}, and the $O_{II}-O_{II}$ distances in the SO_4 tetrahedra are 2.51, 2.51, and 2.60 Å, respectively. These parameters were all determined at room temperature. Although the octahedron of oxygens surrounding the cobalt is strongly distorted as is shown in Fig. 3, the tetrahedron of oxygens about the sulfur is only very slightly distorted. Further, each O_{II} is bonded to two cobalts and one sulfur, whereas each O_I is bonded to only one cobalt and one sulfur. The CoO_6 octahedron is tilted as well as being distorted. It is of great importance to notice that the adjacent octahedra along the crystal c axis are tilted with respect to one another (the axis of rotation being along a), whereas the octahedra surrounding the cobalts in the *ab* plane have the same orientation. Comparing Figs. 1 and 2, we see that the orientations of the magnetic moments of the cobalt ions and the corresponding oxygen octahedra are identical, save for the magnitudes of the tilt angles. The angle between the Co−O_I bond

TABLE I. Position parameters of atoms in α-$CoSO_4$.

Atom	x	y	z
Co	0	0	0
S	0	0.361	0.250
O_I	0	0.250	0.058
O_{II}	0.250	0.472	0.250

TABLE II. Interatomic distances in α-$CoSO_4$.

Atom	Neighbor	Coordination number	Distance (Å)
Co	O_I	2	2.01
Co	O_{II}	4	2.10
S	O_I	2	1.53
S	O_{II}	2	1.57

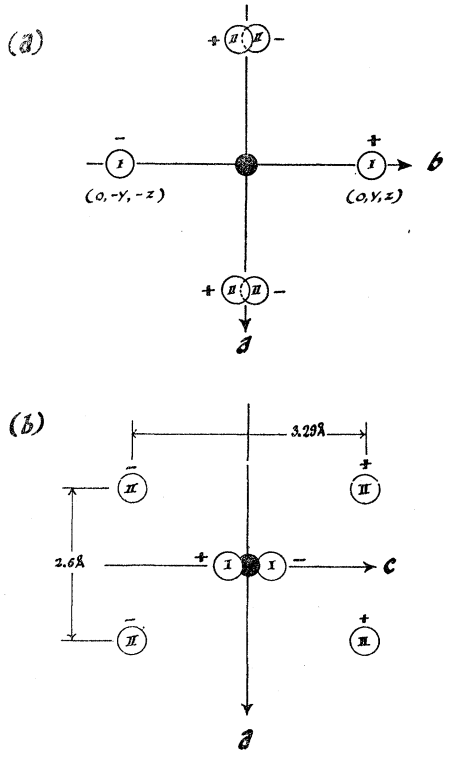

FIG. 3. The octahedral environment of the cobalt ions: (a) projection onto the *ab* plane; (b) projection onto the *ac* plane. The + and − denote above and below the plane of the paper.

[13] M. J. Coing-Boyat, Compt. Rend. 248, 2109 (1959).
[14] P. A. Kokkoros and P. J. Rentzeperis, Acta Cryst. 11, 361 (1958).
[15] A. S. Borovik-Romanov and N. M. Kreines, Zh. Eksperim. i Teor. Fiz. 33, 1119 (1957) [English transl.: Soviet Phys.—JETP 6, 862 (1958)].
[16] N. M. Kreines, Zh. Eksperim. i Teor. Fiz. 35, 1391 (1958) [English transl.: Soviet Phys.—JETP 8, 972 (1959)].
[17] *International Tables for X-Ray Crystallography* (The Kynoch Press, Birmingham, England, 1952).

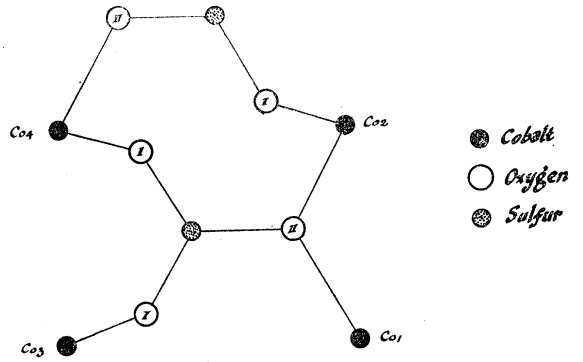

FIG. 4. A projection of the atoms involved in some of the important exchange paths onto the plane containing the four inequivalent cobalt ions.

and the b axis is 10.9°, and the angle between the plane containing the four O_{II}'s and the ca plane is 7.7°. If the octahedron were tilted but not distorted, these two angles would be equal; however, even if these angles were the same, the octahedron could still be distorted. One can consider a larger environment of the cobalt ion in which case we see that it is actually sitting in a distorted octahedron of (SO_4^{--}) tetrahedra. In this case we find 29.9° and 33.8°, respectively, for the angles given above, where the angles are now between the Co−S direction and the b axis, and between the plane containing the 4 sulfurs (associated with the Co−O_{II} bonds) and the ca plane. For comparison, the cant angle of the magnetic moments is 25° in the same sense.

It is convenient to label the four cobalt ions at the positions (0,0,0), (0,0,$\frac{1}{2}$), ($\frac{1}{2}$,$\frac{1}{2}$,0), and ($\frac{1}{2}$,$\frac{1}{2}$,$\frac{1}{2}$) in the chemical unit cell with the numbers 1, 2, 3, and 4, respectively, as shown in Fig. 1. In Table III, we can then write down those exchange paths between the cobalts which are likely to be the most important.

Some of these paths are shown in Fig. 4. Exchange paths of the type Co−O−O−Co in which the two oxygens belong to a given SO_4 tetrahedron have been ignored since the oxygen ions are bonded primarily to the sulfur and the cobalt ions and not to themselves.

TABLE III. Exchange paths in α-$CoSO_4$.

Cobaltions	Paths	Number of neighbors, Z_{ij}
Co_1-Co_2 Co_3-Co_4	Co−O_{II}−Co Co−O_{II}−Co Co−O_I−S−O_I−Co	2
Co_1-Co_3 Co_2-Co_4	Co−O_I−S−O_{II}−Co Co−O_{II}−S−O_I−Co	4
Co_1-Co_4 Co_2-Co_3	Co−O_I−S−O_{II}−Co	8
Co_1-Co_1 Co_2-Co_2 Co_3-Co_3 Co_4-Co_4	Co−O_{II}−S−O_{II}−Co Co−O_{II}−S−O_{II}−Co	2

The S−O bond is a very strong one and its predominant character is covalent; the Co−O bond is comparatively weak and is mostly ionic.

III. TWO-SUBLATTICE MODEL

Before embarking upon a long and tedious calculation using the four sublattices necessary to treat the α-$CoSO_4$ problem, it is instructive and illuminating to first consider a simpler problem involving only two sublattices. The purpose of introducing this model is to show that the anisotropy in the g values of the Co^{++} ions can give rise to large canting angles of the magnetic moments if the axes of the g tensors are tilted with respect to one another. The two sublattices are formed from adjacent cobalt ions located in two sites of distorted octahedra whose axes are tilted with respect to one another. In Fig. 5(a) the xyz coordinate system coincides with the crystal system and the $x_i'y_i'z_i'$ system coincides with the principal axes of the g tensor of the ith cobalt ion. Since, at this time, we are just seeking to show the effects of the anisotropy of the g tensors, we shall describe the system in terms of the true spin with the *isotropic* superexchange Hamiltonian

$$\mathcal{H}=-J\mathbf{S}_1\cdot\mathbf{S}_2, \tag{2}$$

where J is positive. It will be shown in Sec. IX, that the true spin magnitudes are anisotropic if the octahedral environment of the cobalt ions is distorted; thus, although Eq. (2) is isotropic in the above form, it can give rise to much anisotropy when its effects are considered within a ground manifold whose nature is dictated by the larger perturbations of the crystal field and the spin-orbit coupling. The problem is greatly simplified if we put all the anisotropy into some effective exchange constants and work with isotropic spin variables. This can be done by introducing the fictitious spin.[18] The magnetic properties of a system are described by those low-lying states which involve spin and orbital angular momentum reorientations. In cobalt, at low temperatures, the only energy level which is effectively populated is the ground Kramers' doublet (see Sec. IX and Fig. 9) for which the two states can be denoted by $|a\rangle$ and $|b\rangle$. Thus we need consider only these two states when evaluating the low-temperature magnetic properties of the crystal. For a doublet state the fictitious spin is $s=\frac{1}{2}$ so that $2s+1=2$. We shall henceforth denote the true spin with an *upper case S* and the fictitious spin with a *lower case s*.

The g values are defined by considering the Zeeman Hamiltonian

$$\mathcal{H}_z=\beta\mathbf{H}\cdot(\mathbf{L}+2\mathbf{S}), \tag{3}$$

within the states $|a\rangle$ and $|b\rangle$, and writing down an equivalent Zeeman operator

$$\mathcal{H}_z=\beta\mathbf{H}\cdot\mathbf{g}\cdot\mathbf{s}\equiv\beta(g_{x'}H_{x'}s_{x'}+g_{y'}H_{y'}s_{y'}+g_{z'}H_{z'}s_{z'}), \tag{3'}$$

[18] B. Bleaney and K. W. H. Stevens, Rept. Progr. Phys. **16**, 108 (1953).

operating with the states $|+\frac{1}{2}\rangle$ and $|-\frac{1}{2}\rangle$. Identifying corresponding matrix elements, the familiar relations[18] are obtained:

$$g_{x'}=2\langle b|L_{x'}+2S_{x'}|a\rangle,$$
$$g_{y'}=-2i\langle b|L_{y'}+2S_{y'}|a\rangle,$$
$$g_{z'}=2\langle a|L_{z'}+2S_{z'}|a\rangle.$$

The g values may be split up into orbital and spin parts and

$$g=g^L+g^S,$$
$$\mathbf{S}_i=\tfrac{1}{2}g_i{}^S\mathbf{s}_i,\quad i=x',y',z'. \tag{4}$$

Equation (2), which is expressed in terms of the true spins can be written in terms of the fictitious spins if we transform $\mathbf{S}_1$ and $\mathbf{S}_2$ to the $x'y'z'$ system (Fig. 5) so that we may use Eq. (4). The transformation for $\mathbf{S}_1$ is

$$S_{ix}=S_{ix'},$$
$$S_{iy}=S_{iy'}\cos\theta+S_{iz'}\sin\theta, \tag{5}$$
$$S_{iz}=-S_{iy'}\sin\theta+S_{iz'}\cos\theta,$$

and similar equations hold for $\mathbf{S}_2$ with θ replaced by $-\theta$. Thus applying Eqs. (5) and (4) to (2), we find

$$\mathcal{H}=-\tfrac{1}{4}J[(g_{x'}{}^S)^2s_{1x'}s_{2x'}+(g_{y'}{}^S)^2\cos2\theta s_{1y'}s_{2y'}+(g_{z'}{}^S)^2\cos2\theta s_{1z'}s_{2z'}-g_{y'}{}^Sg_{z'}{}^S\sin2\theta\times(s_{1y'}s_{2z'}-s_{1z'}s_{2y'})]. \tag{6}$$

The last term on the right is antisymmetric in the fictitious spin and gives rise to a canting of $\mathbf{s}_1$ and $\mathbf{s}_2$. (To verify that the antisymmetric term is not a spurious effect due to expressing the Hamiltonian in terms of two coordinate systems which are tilted with respect to one another, one may transform the fictitious spins back to the crystal xyz axes. If this is done an antisymmetric term of the form $\mathbf{D}\cdot\mathbf{s}_1\times\mathbf{s}_2$ will be seen to exist.)

To determine the equilibrium directions of the fictitious spins below the ordering temperature, we define the $x_1''y_1''z_1''$ and $x_2''y_2''z_2''$ coordinate systems shown in Fig. 5(a) such that in equilibrium $\langle\mathbf{s}_1\rangle$ and $\langle\mathbf{s}_2\rangle$ point along the y_1'' and y_2'' axes. The transformations are

$$s_{1x'}=s_{1x''},$$
$$s_{1y'}=s_{1y''}\cos\varphi_s+s_{1z''}\sin\varphi_s, \tag{7}$$
$$s_{1z'}=-s_{1y''}\sin\varphi_s+s_{1z''}\cos\varphi_s,$$

and again we get the transformation on $\mathbf{s}_2'$ by changing the sign of φ_s. In the $x''y''z''$ systems $s_{y''}$ must be a constant of the motion.[19] Thus by performing the transformation (7) on Eq. (6) and using

$$i\hbar ds_{y''}/dt=[s_{y''},\mathcal{H}]\equiv0, \tag{8}$$

we find for the equilibrium angle φ_s of the fictitious spins

$$\tan2\varphi_s=-\frac{2g_{y'}{}^Sg_{z'}{}^S\tan2\theta}{(g_{y'}{}^S)^2+(g_{z'}{}^S)^2}. \tag{9}$$

Finally, to find the equilibrium direction of the magnetic moments, we note that by projecting $s_{1y''}$ onto the single-primed axis

$$m_{1z'}=\beta g_{z'}s_{1z'}=\beta g_{z'}s_{1y''}\sin\varphi_s,$$
$$m_{1y'}=\beta g_{y'}s_{1y'}=\beta g_{y'}s_{1y''}\cos\varphi_s. \tag{10}$$

If φ_m is the angle between the magnetic moment and the single-primed y axis [Fig. 5(b)], then

$$\tan\varphi_m=(g_{z'}/g_{y'})\tan\varphi_s, \tag{11}$$

and in equilibrium the value of the magnetic moment

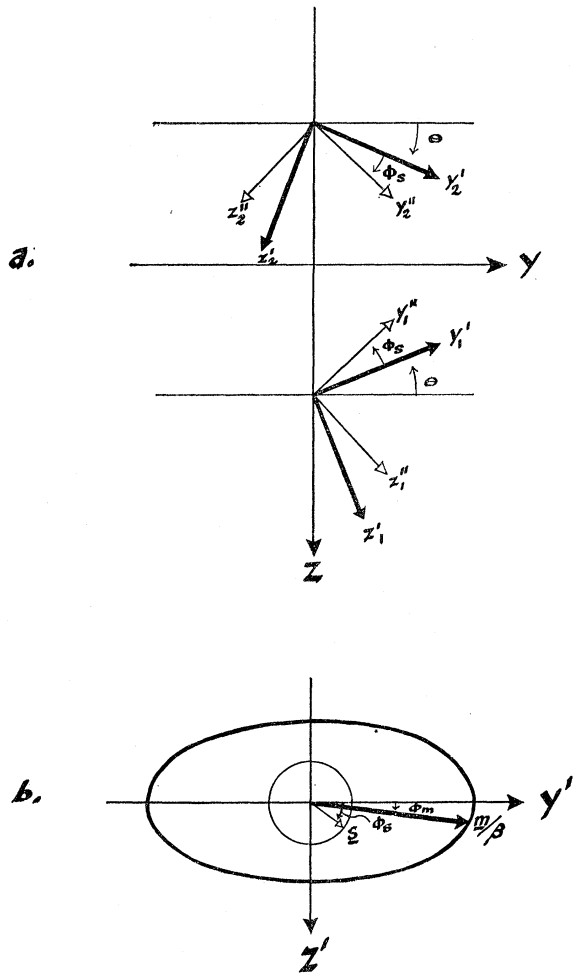

FIG. 5. (a) The various coordinate systems in the two-sublattice model. The xyz system is the crystal system; the $x'y'z'$ the system in which the g tensor is diagonal; and the $x''y''z''$ the system in which $\mathbf{s}$ lies along y'' in equilibrium. (b) The relationship between the fictitious spin $\mathbf{s}$ and the magnetic moment $\mathbf{m}$.

[19] J. H. Van Vleck, Phys. Rev. 74, 1168 (1948).

TABLE IV. Permutation of the Co^{++} ions under the operations of the space group.[a]

Co site	$4I_1$	$4I_2$	$4C_{2x}$	$4C_{2x}^{sc}$	$2\sigma_x$	$2\sigma_x^{gl}$	$4C_{2y}$	$4C_{2y}^{sc}$	$2\sigma_y^{gl\,1}$	$2\sigma_y^{gl\,2}$	$4C_{2z}^{sc\,1}$	$4C_{2z}^{sc\,2}$	$2\sigma_z$	$2\sigma_z^{gl}$
$Co_1(0,0,0)$	1	3	1	3	1	3	2	4	2	4	2	4	2	4
$Co_2(0,0,\frac{1}{2})$	2	4	2	4	2	4	1	3	1	3	1	3	1	3
$Co_3(\frac{1}{2},\frac{1}{2},0)$	3	1	3	1	3	1	4	2	4	2	4	2	4	2
$Co_4(\frac{1}{2},\frac{1}{2},\frac{1}{2})$	4	2	4	2	4	2	3	1	3	1	3	1	3	1

[a] I_1 and I_2 stand for inversion, C_{2i} is rotation by π about the ith axis, and σ_i is reflection in a plane perpendicular to the ith axis. Superscripts sc and gl refer to screw and glide operations, respectively.
In a notation in which the bottom row shows the effect of the operator outside of the parentheses on the top row, we note:

$$I\begin{pmatrix} s_x & s_y & s_z \\ s_x & s_y & s_z \end{pmatrix} \qquad T\begin{pmatrix} s_x & s_y & s_z \\ s_x & s_y & s_z \end{pmatrix} \qquad (T=\text{Translation})$$

$$C_{2x}\begin{pmatrix} s_x & s_y & s_z \\ s_x & -s_y & -s_z \end{pmatrix} \qquad C_{2y}\begin{pmatrix} s_x & s_y & s_z \\ -s_x & s_y & -s_z \end{pmatrix} \qquad C_{2z}\begin{pmatrix} s_x & s_y & s_z \\ -s_x & -s_y & s_z \end{pmatrix}$$

$$\sigma_x\begin{pmatrix} s_x & s_y & s_z \\ s_x & -s_y & -s_z \end{pmatrix} \qquad \sigma_y\begin{pmatrix} s_x & s_y & s_z \\ -s_x & s_y & -s_z \end{pmatrix} \qquad \sigma_z\begin{pmatrix} s_x & s_y & s_z \\ -s_x & -s_y & s_z \end{pmatrix}.$$

is given by

$$m(\varphi_s)=\beta g(\varphi_s)s_{y''} =\beta[g_{y'}^2\cos^2\varphi_s+g_{z'}^2\sin^2\varphi_s]^{1/2}s_{y''}. \quad (12)$$

The magnetic moment defined by Eq. (12) is that which would be measured in a neutron diffraction experiment. The value of $s_{y''}$ is $\frac{1}{2}$ at $T=0$; for $T\neq 0$, one must use the proper statistical average. It is to be noted that if $g_{y'}\geq g_{z'}$, then **m** always lies between the equilibrium direction of the fictitious spin y'' and the y' axis. The magnitude of **m** must also satisfy the inequality

$$g_{y'}\geq 2m/\beta\geq g_{z'}. \quad (13)$$

We now consider two limiting cases:

(a) The g tensors are not tilted with respect to each other. In this case $\theta=0$ and from Eq. (9) $\varphi_s=0$ so that there is no canting.

(b) The g tensor is isotropic. From Eq. (9) we find $\tan 2\varphi_s=-\tan 2\theta$ or $\varphi_s=-\theta$ and again there is no canting.

To get an idea of the order of magnitude of the canting due to the anisotropic g tensor we use some typical values in Eq. (9):

$$g_{y'}=7, \quad g_{x'}=g_{z'}=3, \quad g_{y'}{}^S=5, \quad g_{z'}{}^S=g_{x'}{}^S=2.5. \quad (14)$$

If $\theta=20°$, then $\varphi_s\approx -17°$ and from Eq. (11) we find $\varphi_m=-7.5°$. The angle of cant away from the y axis is $\theta+\varphi_m=12.5°$. We conclude that the anisotropy of the g tensor alone can give rise to large canting angles.

IV. THE HAMILTONIAN FOR THE FOUR-SUBLATTICE CASE

As can be seen from Table III or Figs. 2 and 4, the principal exchange paths of α-$CoSO_4$ are many and varied. Each cobalt spin on a given sublattice not only interacts with its nearest neighbors on the other three sublattices, but also has an intrasublattice interaction with its nearest neighbors along the crystal a axis. For an initial attempt to write down a Hamiltonian which describes the magnetic structure, one might assume that the exchange between the true spins is isotropic, attributing the anisotropy and canting to the g-tensor effects as was shown in the previous section. Although this approach yields the proper magnetic symmetry, a consideration of the stability shows that the equilibrium direction of the magnetic moments must always be between the crystal b axis (y axis in the notation of Sec. III) and y' axis (also defined in Sec. III), no matter what combination of ferromagnetic and antiferromagnetic exchange integrals is used between the different spins. If the y' axis of the g tensor were to coincide with the Co—O_I bond, then the angle θ between the y and y' axis would be $\sim 11°$, and since the angle between the y axis and the magnetic moment is $\sim 25°$, we would not be able to stabilize the magnetic structure observed for α-$CoSO_4$. On the other hand, if the y' axis of the g tensor were to coincide with the Co—S direction, the angle θ would be $\sim 30°$, and one might be able to use an isotropic exchange model. Actually, the charge distribution in the sulfate tetrahedra is complex and unknown; consequently, we cannot determine the angle θ and therefore we shall consider it as a variable for the present.

Our program in this section is thus to write down the most general Hamiltonian taking into account all exchange interactions which have been previously mentioned. We shall then show how it is possible to simplify the Hamiltonian enormously by considering the space group of the crystal.

Labeling the cobalt ions or spins as is shown in Fig. 1, the exchange Hamiltonian can be written:

$$\mathcal{H}=\mathcal{H}^{12}+\mathcal{H}^{13}+\mathcal{H}^{14}+\mathcal{H}^{23}+\mathcal{H}^{24}+\mathcal{H}^{34} +\mathcal{H}^{11}+\mathcal{H}^{22}+\mathcal{H}^{33}+\mathcal{H}^{44}, \quad (15a)$$

where, if the crystal coordinate system is used,

$$\mathcal{H}^{ij}=J_{xx}{}^{ij}s_{ix}s_{jx}+J_{yy}{}^{ij}s_{iy}s_{jy}+J_{zz}{}^{ij}s_{iz}s_{jz} +K_{xy}{}^{ij}(s_{ix}s_{jy}+s_{iy}s_{jx})+K_{yz}{}^{ij}(s_{iy}s_{jz}+s_{iz}s_{jy}) +K_{zx}{}^{ij}(s_{iz}s_{jx}+s_{ix}s_{jz})+L_{xy}{}^{ij}(s_{ix}s_{jy}-s_{iy}s_{jx}) +L_{yz}{}^{ij}(s_{iy}s_{jz}-s_{iz}s_{jy})+L_{zx}{}^{ij}(s_{iz}s_{jx}-s_{ix}s_{jz}). \quad (15b)$$

This is a completely general expression for the quadratic exchange interaction between two spins. The spin components in this expression are those of an isotropic fictitious spin of $\frac{1}{2}$. The coefficients of the spin operators in (15b) will contain effects due to isotropic real spin

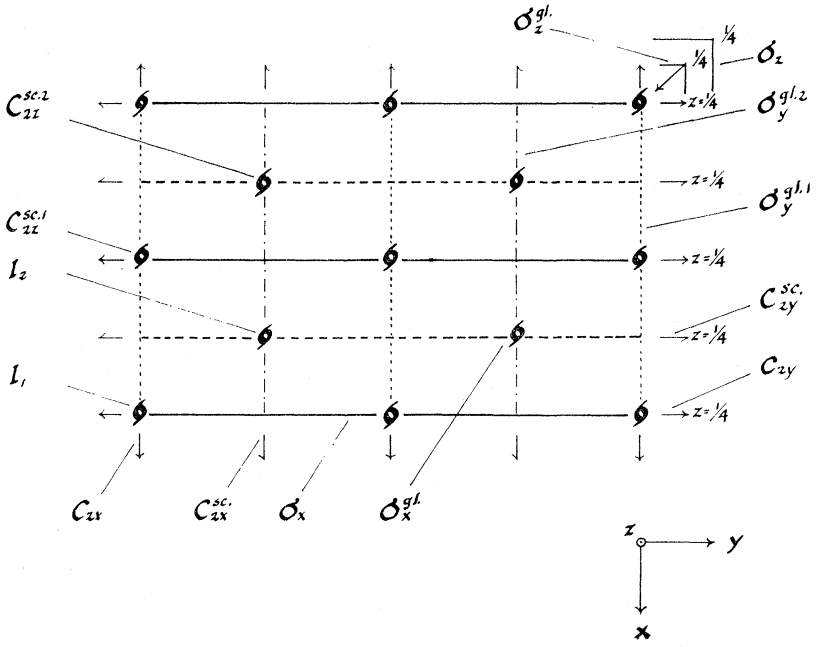

FIG. 6. The symmetry elements of space group D_{2h}^{17}. Most operations are self-evident. The inversion I_2 is located between Co_1 and Co_3, etc.; the translation in $\sigma_y^{gl\,1}$ is $z/2$; in $\sigma_y^{gl\,2}$ is $(a+c)/2$; and in σ_z^{gl} is $(a+b)/2$.

exchange, symmetric and antisymmetric anisotropic real spin exchange, and g-value anisotropy. For a spin of $\frac{1}{2}$, there can be no real single-ion anisotropy effects since all squares of spin-$\frac{1}{2}$ matrices are multiples of the unit matrix, and thus do not exhibit anisotropy effects. In our case, the intrasublattice exchange terms $\mathcal{H}^{ii}$ will produce effects which look like single-ion anisotropy on a four-sublattice model. The pairs of spins referred to in the expression for $\mathcal{H}^{ii}$ in (15b) are never identical, so that terms such as $s_{ix}s_{ix}$ should actually be written $s_{ix}s_{i'x}$. In order to limit the number of sublattices to four, we have set $s_{i'x}=s_{ix}$. Later, in taking the commutator of $\mathbf{s}_i$ with $\mathcal{H}^{ii}$, we must remember this since $\mathbf{s}_i$ commutes with all components of $\mathbf{s}_{i'}$.

The Hamiltonian (15) has 90 parameters. Next, we write down the elements of the space group D_{2h}^{17} (Ref. 17), their spatial positions being shown in Fig. 6. In Table IV we show how the four cobalt ions are permuted by the space group operations. Now let us consider the information we obtain by operating with the various elements of the space group on the Hamiltonian, Eq. (15), which must remain invariant. Noting that it is not necessary to consider the operations involving reflection as each of these operations can be paired off with a twofold rotation which has exactly the same effect on the magnetic Hamiltonian, we find:

I_1: provides no information,

I_2: $J^{12}=J^{34}$; $K^{12}=K^{34}$; $L^{12}=L^{34}$; $J^{14}=J^{32}$; $K^{14}=K^{32}$; $L^{14}=L^{32}$

$J^{11}=J^{33}$; $K^{11}=K^{33}$; $J^{22}=J^{44}$; $K^{22}=K^{44}$; $L^{13}=L^{24}=0$.

In a similar way, we continue to apply the symmetry operations of the crystal to the Hamiltonian to find relations between the exchange parameters. Taking all of these relations into account, we are able to write down the most general quadratic exchange Hamiltonian allowed by the symmetry of the crystal:

$$
\begin{aligned}
\mathcal{H}^{12}&=J_{xx}^{12}s_{1x}s_{2x}+J_{yy}^{12}s_{1y}s_{2y}+J_{zz}^{12}s_{1z}s_{2z}+L_{yz}^{12}(s_{1y}s_{2z}-s_{1z}s_{2y}),\\
\mathcal{H}^{13}&=J_{xx}^{13}s_{1x}s_{3x}+J_{yy}^{13}s_{1y}s_{3y}+J_{zz}^{13}s_{1z}s_{3z}+K_{yz}^{13}(s_{1y}s_{3z}+s_{1z}s_{3y}),\\
\mathcal{H}^{14}&=J_{xx}^{14}s_{1x}s_{4x}+J_{yy}^{14}s_{1y}s_{4y}+J_{zz}^{14}s_{1z}s_{4z}+L_{yz}^{14}(s_{1y}s_{4z}-s_{1z}s_{4y}),\\
\mathcal{H}^{23}&=J_{xx}^{14}s_{2x}s_{3x}+J_{yy}^{14}s_{2y}s_{3y}+J_{zz}^{14}s_{2z}s_{3z}-L_{yz}^{14}(s_{2y}s_{3z}-s_{2z}s_{3y}),\\
\mathcal{H}^{24}&=J_{xx}^{13}s_{2x}s_{4x}+J_{yy}^{13}s_{2y}s_{4y}+J_{zz}^{13}s_{2z}s_{4z}-K_{yz}^{13}(s_{2y}s_{4z}+s_{2z}s_{4y}),\\
\mathcal{H}^{34}&=J_{xx}^{12}s_{3x}s_{4x}+J_{yy}^{12}s_{3y}s_{4y}+J_{zz}^{12}s_{3z}s_{4z}+L_{yz}^{12}(s_{3y}s_{4z}-s_{3z}s_{4y}),\\
\mathcal{H}^{11}&=J_{xx}^{11}s_{1x}^{2}+J_{yy}^{11}s_{1y}^{2}+J_{zz}^{11}s_{1z}^{2}+K_{yz}^{11}(s_{1y}s_{1z}+s_{1z}s_{1y}),\\
\mathcal{H}^{22}&=J_{xx}^{11}s_{2x}^{2}+J_{yy}^{11}s_{2y}^{2}+J_{zz}^{11}s_{2z}^{2}-K_{yz}^{11}(s_{2y}s_{2z}+s_{2z}s_{2y}),\\
\mathcal{H}^{33}&=J_{xx}^{11}s_{3x}^{2}+J_{yy}^{11}s_{3y}^{2}+J_{2z}^{11}s_{3z}^{2}+K_{yz}^{11}(s_{3y}s_{3z}+s_{3z}s_{3y}),\\
\mathcal{H}^{44}&=J_{xx}^{11}s_{4x}^{2}+J_{yy}^{11}s_{4y}^{2}+J_{zz}^{11}s_{4z}^{2}-K_{yz}^{11}(s_{4y}s_{4z}+s_{4z}s_{4y}).
\end{aligned}
\tag{16}
$$

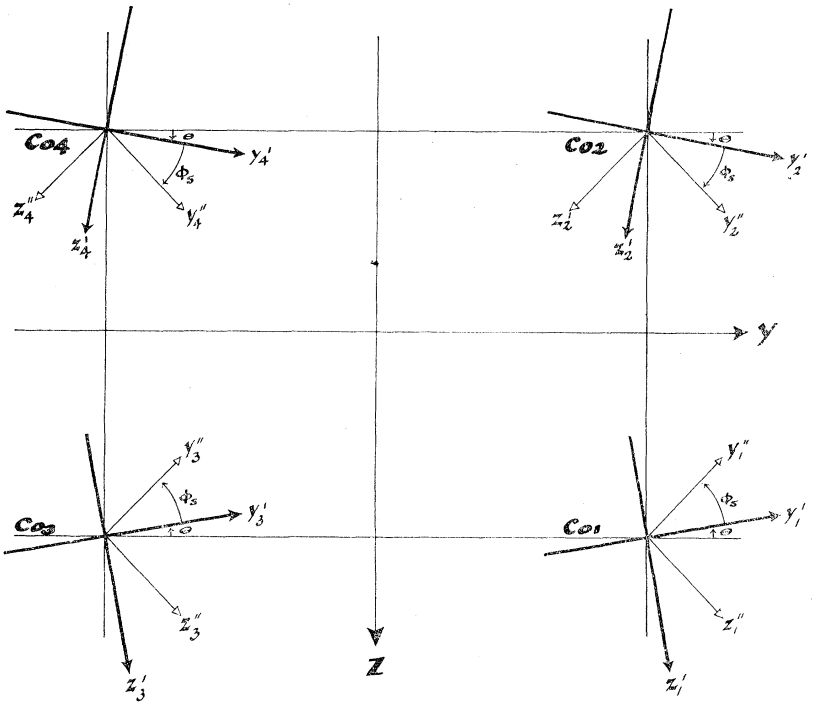

FIG. 7. The various coordinate systems used in describing α-$CoSO_4$. Their significance is given in the text.

We see that this Hamiltonian only allows canting in the yz plane and that there is no canting interaction between either $\mathbf{s}_1$ and $\mathbf{s}_3$ or $\mathbf{s}_2$ and $\mathbf{s}_4$ so that they will be either parallel or antiparallel. All of this is consistent with the magnetic symmetry found by neutron diffraction.

Although we have now obtained a Hamiltonian (16) which must describe the magnetic properties of the system, we still do not have the most convenient form of the Hamiltonian with which to attack the problem. It is a great convenience if we choose different axes for each spin in such a way that the ground-state magnetic order (Fig. 1) is naturally described by the system of axes. Let us transform (16) to the double-primed system of axes shown in Fig. 7. In this diagram, the single-primed axes are the principal axes of the cobalt g tensor. The double-primed axes describe the equilibrium configuration of the cobalt fictitious spins so that at absolute zero

$$\langle s_{1y''}\rangle=\langle s_{2y''}\rangle=-\langle s_{3y''}\rangle=-\langle s_{4y''}\rangle=s, \qquad (17)$$

where $s=\frac{1}{2}$ is the fictitious spin.

On transforming (16) to the double-primed coordinate system, we obtain equations identical in form to (16) but with $x''y''z''$ replacing xyz throughout. For example,

$$\mathcal{H}^{12}=J_{x''x''}{}^{12}s_{1x''}s_{2x''}+J_{y''y''}{}^{12}s_{1y''}s_{2y''}+J_{z''z''}{}^{12}s_{1z''}s_{2z''}+L_{y''z''}{}^{12}(s_{1y''}s_{2z''}-s_{1z''}s_{2y''}). \qquad (18)$$

The new double-primed coefficients are functions of the unprimed coefficients and of θ and φ_s; at present we are not particularly interested in these functions. The behavior of the system can be described either by the 16 independent parameters of Eqs. (16) or by the 16 double primed parameters of Eqs. (18). It will be seen that it is much more convenient to describe the system in terms of the latter set.

The angle φ_s of our transformation is determined by the fact that the double-primed equations of the form (18) must provide a stable configuration with the fictitious spins pointing along the y'' directions. Taking the commutator, Eq. (8), of $s_{1y''}$ with the Hamiltonian, it is easily shown that the condition is

$$L_{y''z''}{}^{12}+K_{y''z''}{}^{13}-L_{y''z''}{}^{14}-K_{y''z''}{}^{11}=0. \qquad (19)$$

V. THE RESONANCE FREQUENCIES AND NORMAL MODES

It is desirable to treat this problem quantum mechanically, since in anisotropic systems a correct semiclassical treatment is not always apparent. To write down the equations of motion we use

$$i\hbar\dot{\mathbf{s}}=[\mathbf{s},\mathcal{H}] \qquad (20)$$

and

$$[s_x,s_y]=is_z, \text{ etc.} \qquad (21)$$

The equations are linearized by assuming small oscillations about the configuration described by (17) and letting the x'' and z'' components of spin have time dependence $\exp(-i\omega t)$. If $p=(i\hbar\omega)/s$, the elements of

the resonance matrix are

	$s_{1x''}$	$s_{2x''}$	$s_{3x''}$	$s_{4x''}$	$s_{1z''}$	$s_{2z''}$	$s_{3z''}$	$s_{4z''}$
$s_{1x''}$	p	0	0	0	$-J_0$	$-J_{z''z''}{}^{12}$	$-J_{z''z''}{}^{13}$	$-J_{z''z''}{}^{14}$
$s_{2x''}$	0	p	0	0	$-J_{z''z''}{}^{12}$	$-J_0$	$-J_{z''z''}{}^{14}$	$-J_{z''z''}{}^{13}$
$s_{3x''}$	0	0	p	0	$J_{z''z''}{}^{13}$	$J_{z''z''}{}^{14}$	J_0	$J_{z''z''}{}^{12}$
$s_{4x''}$	0	0	0	p	$J_{z''z''}{}^{14}$	$J_{z''z''}{}^{13}$	$J_{z''z''}{}^{12}$	J_0
$s_{1z''}$	J_0	$J_{x''x''}{}^{12}$	$J_{x''x''}{}^{13}$	$J_{x''x''}{}^{14}$	p	0	0	0
$s_{2z''}$	$J_{x''x''}{}^{12}$	J_0	$J_{x''x''}{}^{14}$	$J_{x''x''}{}^{13}$	0	p	0	0
$s_{3z''}$	$-J_{x''x''}{}^{13}$	$-J_{x''x''}{}^{14}$	$-J_0$	$-J_{x''x''}{}^{12}$	0	0	p	0
$s_{4z''}$	$-J_{x''x''}{}^{14}$	$-J_{x''x''}{}^{13}$	$-J_{x''x''}{}^{12}$	$-J_0$	0	0	0	p

, (22a)

where

$$-J_0=J_{y''y''}{}^{12}-J_{y''y''}{}^{13}-J_{y''y''}{}^{14}+J_{y''y''}{}^{11}-J_{z''z''}{}^{11}. \tag{22b}$$

The solutions to the associated secular equation are

$$\omega_{1,2}{}^2=(s^2/\hbar^2)(J_0+J_{x''x''}{}^{12}+J_{x''x''}{}^{13}+J_{x''x''}{}^{14})(J_0+J_{z''z''}{}^{12}-J_{z''z''}{}^{13}-J_{z''z''}{}^{14}), \tag{23a}$$

$$\omega_{3,4}{}^2=(s^2/\hbar^2)(J_0+J_{z''x''}{}^{12}-J_{x''x''}{}^{13}-J_{x''x''}{}^{14})(J_0+J_{z''z''}{}^{12}+J_{z''z''}{}^{13}+J_{z''z''}{}^{14}), \tag{23b}$$

$$\omega_{5,6}{}^2=(s^2/\hbar^2)(J_0-J_{x''x''}{}^{12}-J_{x''x''}{}^{13}+J_{x''x''}{}^{14})(J_0-J_{z''z''}{}^{12}+J_{z''z''}{}^{13}-J_{z''z''}{}^{14}), \tag{23c}$$

$$\omega_{7,8}{}^2=(s^2/\hbar^2)(J_0-J_{x''x''}{}^{12}+J_{x''x''}{}^{13}-J_{x''x''}{}^{14})(J_0-J_{z''z''}{}^{12}-J_{z''z''}{}^{13}+J_{z''z''}{}^{14}). \tag{23d}$$

We have eight roots, only half of which are significant since the $\pm\omega$ solutions are physically identical. The corresponding normal modes are described by the matrix which diagonalizes (22a), namely:

	ω_1	ω_2	ω_3	ω_4	ω_5	ω_6	ω_7	ω_8
$s_{1x''}$	1	1	1	1	1	1	1	1
$s_{2x''}$	1	1	1	1	−1	−1	−1	−1
$s_{3x''}$	1	1	−1	−1	−1	−1	1	1
$s_{4x''}$	1	1	−1	−1	1	1	−1	−1
$s_{1z''}$	$-i\mu$	$i\mu$	$-i\nu$	$i\nu$	$-i\sigma$	$i\sigma$	$-i\tau$	$i\tau$
$s_{2z''}$	$-i\mu$	$i\mu$	$-i\nu$	$i\nu$	$i\sigma$	$-i\sigma$	$i\tau$	$-i\tau$
$s_{3z''}$	$i\mu$	$-i\mu$	$-i\nu$	$i\nu$	$-i\sigma$	$i\sigma$	$i\tau$	$-i\tau$
$s_{4z''}$	$i\mu$	$-i\mu$	$-i\nu$	$i\nu$	$i\sigma$	$-i\sigma$	$-i\tau$	$i\tau$

, (24)

where

$$\mu=\left(\frac{J_0+J_{x''x''}{}^{12}+J_{x''x''}{}^{13}+J_{x''x''}{}^{14}}{J_0+J_{z''z''}{}^{12}-J_{z''z''}{}^{13}-J_{z''z''}{}^{14}}\right)^{1/2}, \tag{25a}$$

$$\nu=\left(\frac{J_0+J_{x''x''}{}^{12}-J_{x''x''}{}^{13}-J_{x''x''}{}^{14}}{J_0+J_{z''z''}{}^{12}+J_{z''z''}{}^{13}+J_{z''z''}{}^{14}}\right)^{1/2}, \tag{25b}$$

$$\sigma=\left(\frac{J_0-J_{x''x''}{}^{12}-J_{x''x''}{}^{13}+J_{x''x''}{}^{14}}{J_0-J_{z''z''}{}^{12}+J_{z''z''}{}^{13}-J_{z''z''}{}^{14}}\right)^{1/2}, \tag{25c}$$

$$\tau=\left(\frac{J_0-J_{x''x''}{}^{12}+J_{x''x''}{}^{13}-J_{x''x''}{}^{14}}{J_0-J_{z''z''}{}^{12}-J_{z''z''}{}^{13}+J_{z''z''}{}^{14}}\right)^{1/2}. \tag{25d}$$

These normal modes are shown in Fig. 8 and are similar to those found by Joenk[8] for $CuCl_2\cdot 2H_2O$. From the diagram or (24) we can see that modes $\omega_{1,2}$, $\omega_{3,4}$, and $\omega_{5,6}$ have oscillating moments along the crystal a, c, and b axes, respectively. Hence each will absorb radiation polarized along one axis if it is of the proper frequency, as will be shown in the following section. One can show that the intensity of the line associated with $\omega_{5,6}$ is proportional to the square of the sine of the canting angle, and thus this line disappears in the limit of zero cant. Mode $\omega_{7,8}$ has no oscillating magnetic moment and will be unobservable by the usual experimental techniques. In all of the modes, the tips of the fictitious spins describe elliptical paths about their equilibrium directions, with the ratio of the axes of the ellipses being given by Eqs. (25). We point out that the resonance frequencies (23) are affected by the intrasublattice interaction since it is anisotropic [see (22b)].

VI. THE RF SUSCEPTIBILITIES

The calculation of the rf susceptibilities is complicated by the fact that an external magnetic field interacts with the magnetic moments and the principal axes of the g tensors do not lie along the crystal axes which will be the principal axes of the susceptibility by symmetry. We detail the derivation of the interaction

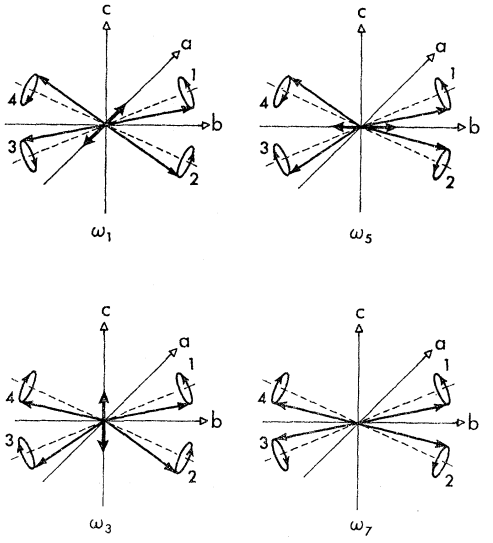

FIG. 8. The normal modes of the fictitious spins. The polarization of the associated oscillating magnetic moments is indicated by the double-headed arrows through the origin.

Hamiltonian for the spin at position 1; the others follow immediately by reversing the angles. With the axes as shown in Fig. 7, let the principal values of the cobalt g tensor along the single-primed axes be $g_{x'}$, $g_{y'}$, and $g_{z'}$. If the interaction of the external magnetic field with $\mathbf{s}_1$ is $\mathcal{H}_1$, then

$$-\mathcal{H}_1=m_{1x'}H_{1x'}+m_{1y'}H_{1y'}+m_{1z'}H_{1z'}. \tag{26}$$

The $H_{1x'}$, etc., are the components of magnetic field observed in the single-primed system of Co_1. For a field applied in the crystal xyz system, the different cobalt ions will see different field components in the primed systems since the axes are tilted with respect to one another. Consequently we distinguish the fields with the numerical subscripts.

We apply the transformations:

$$\begin{aligned} H_{1x'}&=H_x,\\ H_{1y'}&=H_y\cos\theta-H_z\sin\theta,\\ H_{1z'}&=H_y\sin\theta+H_z\cos\theta, \end{aligned} \tag{27}$$

and

$$\begin{aligned} s_{1x'}&=s_{ix''},\\ s_{1y'}&=s_{1y''}\cos\varphi_s+s_{1z''}\sin\varphi_s,\\ s_{1z'}&=-s_{1y''}\sin\varphi_s+s_{1z''}\cos\varphi_s, \end{aligned} \tag{28}$$

and noting that $m_{1x'}=\beta g_{x'}s_{1x'}$, etc., one obtains after a little rearrangement:

$$\begin{aligned} \mathcal{H}_1=&-\beta s_{1x''}g_{x'}H_x\\ &-\beta s_{1y''}[H_y(g_{y'}\cos\varphi_s\cos\theta-g_{z'}\sin\varphi_s\sin\theta)\\ &\quad+H_z(-g_{y'}\cos\varphi_s\sin\theta-g_{z'}\sin\varphi_s\cos\theta)]\\ &-\beta s_{1z''}[H_z(-g_{y'}\sin\varphi_s\sin\theta+g_{z'}\cos\varphi_s\cos\theta)\\ &\quad+H_y(g_{y'}\sin\varphi_s\sin\theta+g_{z'}\cos\varphi_s\sin\theta)]. \end{aligned} \tag{29}$$

$\mathcal{H}_3$ is similar to $\mathcal{H}_1$ whereas $\mathcal{H}_2$ and $\mathcal{H}_4$ are obtained by reversing the signs of θ and φ_s. The additional terms are inserted into the equations of motion (20), and alternatively taking the external field along the crystal x, y, and z axes, the resulting inhomogeneous equations are solved for $s_{1x''}$, etc. The $s_{1x''}$, etc., are then projected into the single-primed axes where they can be converted into magnetic moments by multiplying with the appropriate g value and the Bohr magneton. A further transformation of the magnetic moments into the crystal xyz system then gives the susceptibilities:

$$\chi_x'=\frac{4\beta^2g_x^2s^2}{\hbar^2}\frac{J_0+J_{z''z''}{}^{12}-J_{z''z''}{}^{13}-J_{z''z''}{}^{14}}{(\omega_{1,2}{}^2-\omega^2)}, \tag{30a}$$

$$\chi_y'=\frac{4\beta^2g_{zy}{}^2s^2}{\hbar^2}\frac{(J_0-J_{x''x''}{}^{12}-J_{x''x''}{}^{13}+J_{x''x''}{}^{14})}{(\omega_{5,6}{}^2-\omega^2)}, \tag{30b}$$

$$\chi_z'=\frac{4\beta^2g_{zz}{}^2s^2}{\hbar^2}\frac{(J_0+J_{x''x''}{}^{12}-J_{x''x''}{}^{13}-J_{x''x''}{}^{14})}{(\omega_{3,4}{}^2-\omega^2)}, \tag{30c}$$

where

$$g_x=g_{x'}, \tag{31a}$$

$$g_{zy}=g_{z'}\cos\varphi_s\sin\theta+g_{y'}\sin\varphi_s\cos\theta, \tag{31b}$$

$$g_{zz}=g_{z'}\cos\varphi_s\cos\theta-g_{y'}\sin\varphi_s\sin\theta, \tag{31c}$$

$$g_{yy}=g_{y'}\cos\varphi_s\cos\theta-g_{z'}\sin\varphi_s\sin\theta, \tag{31d}$$

$$g_{yz}=g_{z'}\sin\varphi_s\cos\theta+g_{y'}\cos\varphi_s\sin\theta. \tag{31e}$$

(The expressions for g_{yy} and g_{yz} will be used later in Sec. VIII.)

The integrated absorption may be computed, assuming a narrow linewidth, by applying the Kramers-Kronig relations,[20] with the results

$$\chi_x''\Delta\omega=(2\pi g_x{}^2\beta^2s/\hbar)(1/\mu), \tag{32a}$$

$$\chi_y''\Delta\omega=(2\pi g_{zy}{}^2\beta^2s/\hbar)\sigma, \tag{32b}$$

$$\chi_z''\Delta\omega=(2\pi g_{zz}{}^2\beta^2s/\hbar)\nu. \tag{32c}$$

We notice that the mode $\omega_{7,8}$ does not contribute to the absorption as was pointed out in the preceding section.

Using Eqs. (30) and (23), and setting $\omega=0$, we are able to write the components of the static susceptibility at absolute zero:

$$\chi_x'(0)=\frac{4g_x{}^2\beta^2}{(J_0+J_{x''x''}{}^{12}+J_{x''x''}{}^{13}+J_{x''x''}{}^{14})}, \tag{33a}$$

$$\chi_y'(0)=\frac{4g_{zy}{}^2\beta^2}{(J_0-J_{z''z''}{}^{12}+J_{z''z''}{}^{13}-J_{z''z''}{}^{14})}, \tag{33b}$$

$$\chi_z'(0)=\frac{4g_{zz}{}^2\beta^2}{(J_0+J_{z''z''}{}^{12}+J_{z''z''}{}^{13}+J_{z''z''}{}^{14})}. \tag{33c}$$

[20] M. Tinkham, Phys. Rev. 124, 311 (1961).

It should be remarked that these susceptibility results apply to a single chemical unit cell of α-$CoSO_4$ which contains four cobalt ions.

VII. THE NÉEL TEMPERATURE AND THE STABILITY CONDITION

Equation (18) is a convenient form of the Hamiltonian with 16 parameters and 12 spin variables. If a molecular field calculation is performed using this Hamiltonian, we shall obtain 12 values for the ordering temperature $T_N{}^i$ ($i=1, \cdots, 12$), and corresponding to each root there will be a particular ordering configuration.[21] The fact that the ground-state order is known to be as in Fig. 1 will restrict considerably the values that can be assigned to the parameters in Eq. (18). The calculation is most easily carried out if one takes advantage of a useful result (see Appendix) for the Hamiltonian

$$\mathcal{H}=c_x s_x+c_y s_y+c_z s_z. \tag{34}$$

If $(c_x{}^2+c_y{}^2+c_z{}^2)^{1/2}/2kT\ll 1$, then

$$\langle s_i\rangle_T=-c_i/4kT, \quad i=x, y, z, \tag{35}$$

for a spin of $\frac{1}{2}$. Since, in the molecular field approximation, Eq. (18) takes on the form of Eq. (34), we can write down the system of 12 homogeneous linear equations, (35), in the form of a matrix:

$$\mathbf{M}=\begin{array}{c|c|c} & s_{ix''} & s_{iy''}\ s_{iz''} \\ \hline s_{ix''} & \mathbf{A} & \mathbf{0} \\ \hline s_{iy''}\ s_{iz''} & \mathbf{0} & \mathbf{B} \end{array}, \tag{36}$$

where

$$\mathbf{A}=\begin{array}{c|cccc} & \langle s_{1x''}\rangle & \langle s_{2x''}\rangle & \langle s_{3x''}\rangle & \langle s_{4x''}\rangle \\ \hline \langle s_{1x''}\rangle & \gamma+J_{x''x''}{}^{11} & J_{x''x''}{}^{12} & J_{x''x''}{}^{13} & J_{x''x''}{}^{14} \\ \langle s_{2x''}\rangle & J_{x''x''}{}^{12} & \gamma+J_{x''x''}{}^{11} & J_{x''x''}{}^{14} & J_{x''x''}{}^{13} \\ \langle s_{3x''}\rangle & J_{x''x''}{}^{13} & J_{x''x''}{}^{14} & \gamma+J_{x''x''}{}^{11} & J_{x''x''}{}^{12} \\ \langle s_{4x''}\rangle & J_{x''x''}{}^{14} & J_{x''x''}{}^{13} & J_{x''x''}{}^{12} & \gamma+J_{x''x''}{}^{11} \end{array}, \tag{36a}$$

$$\mathbf{B}=\begin{array}{c|cccccccc} & \langle s_{1y''}\rangle & \langle s_{2y''}\rangle & \langle s_{3y''}\rangle & \langle s_{4y''}\rangle & \langle s_{1z''}\rangle & \langle s_{2z''}\rangle & \langle s_{3z''}\rangle & \langle s_{4z''}\rangle \\ \hline \langle s_{1y''}\rangle & \gamma+J_{y''y''}{}^{11} & J_{y''y''}{}^{12} & J_{y''y''}{}^{13} & J_{y''y''}{}^{14} & K_{y''z''}{}^{11} & L_{y''z''}{}^{12} & K_{y''z''}{}^{13} & L_{y''z''}{}^{14} \\ \langle s_{2y''}\rangle & J_{y''y''}{}^{12} & \gamma+J_{y''y''}{}^{11} & J_{y''y''}{}^{14} & J_{y''y''}{}^{13} & -L_{y''z''}{}^{12} & -K_{y''z''}{}^{11} & -L_{y''z''}{}^{14} & -K_{y''z''}{}^{13} \\ \langle s_{3y''}\rangle & J_{y''y''}{}^{13} & J_{y''y''}{}^{14} & \gamma+J_{y''y''}{}^{11} & J_{y''y''}{}^{12} & K_{y''z''}{}^{13} & L_{y''z''}{}^{14} & K_{y''z''}{}^{11} & L_{y''z''}{}^{12} \\ \langle s_{4y''}\rangle & J_{y''y''}{}^{14} & J_{y''y''}{}^{13} & J_{y''y''}{}^{12} & \gamma+J_{y''y''}{}^{11} & -L_{y''z''}{}^{14} & -K_{y''z''}{}^{13} & -L_{y''z''}{}^{12} & -K_{y''z''}{}^{11} \\ \langle s_{1z''}\rangle & K_{y''z''}{}^{11} & -L_{y''z''}{}^{12} & K_{y''z''}{}^{13} & -L_{y''z''}{}^{14} & \gamma+J_{z''z''}{}^{11} & J_{z''z''}{}^{12} & J_{z''z''}{}^{13} & J_{z''z''}{}^{14} \\ \langle s_{2z''}\rangle & L_{y''z''}{}^{12} & -K_{y''z''}{}^{11} & L_{y''z''}{}^{14} & -K_{y''z''}{}^{13} & J_{z''z''}{}^{12} & \gamma+J_{z''z''}{}^{11} & J_{z''z''}{}^{14} & J_{z''z''}{}^{13} \\ \langle s_{3z''}\rangle & K_{y''z''}{}^{13} & -L_{y''z''}{}^{14} & K_{y''z''}{}^{11} & -L_{y''z''}{}^{12} & J_{z''z''}{}^{13} & J_{z''z''}{}^{14} & \gamma+J_{z''z''}{}^{11} & J_{z''z''}{}^{12} \\ \langle s_{4z''}\rangle & L_{y''z''}{}^{14} & -K_{y''z''}{}^{13} & L_{y''z''}{}^{12} & -K_{y''z''}{}^{11} & J_{z''z''}{}^{14} & J_{z''z''}{}^{13} & J_{z''z''}{}^{12} & \gamma+J_{z''z''}{}^{11} \end{array}, \tag{36b}$$

and

$$\gamma=4kT. \tag{37}$$

The matrix $\mathbf{M}$ is diagonalized in the usual way. If $\mathbf{U}^{-1}\mathbf{M}\mathbf{U}$ is diagonal, then the columns of $\mathbf{U}$ are the spin eigenvectors which determine the spin configurations. Twelve distinct roots are obtained in all, with each root corresponding to a different spin configuration and Néel temperature. We shall give only the root for the spin configuration observed by neutron diffraction, which is

$$\gamma_N\equiv 4kT_N=-J_{y''y''}{}^{11}-J_{y''y''}{}^{12}+J_{y''y''}{}^{13}+J_{y''y''}{}^{14}=J_0-J_{z''z''}{}^{11}. \tag{38}$$

VIII. STATIC SUSCEPTIBILITIES ABOVE THE NÉEL TEMPERATURE ON THE MOLECULAR FIELD MODEL

This calculation is completely straightforward, the procedure being the same as in the calculation of the rf susceptibilities. The results are given below:

$$\chi_x(T>T_N)=\frac{4\beta^2 g_x{}^2}{4kT+J_{x''x''}{}^{11}+J_{x''x''}{}^{12}+J_{x''x''}{}^{13}+J_{x''x''}{}^{14}}, \tag{39}$$

[21] P. W. Anderson, Phys. Rev. **79**, 705 (1950).

$$\chi_y(T>T_N)=\frac{4\beta^2[g_{yy}^2(4kT+J_{z''z''}{}^{11}-J_{z''z''}{}^{12}+J_{z''z''}{}^{13}-J_{z''z''}{}^{14})+g_{zy}^2(4kT+J_{y''y''}{}^{11}+J_{y''y''}{}^{12}+J_{y''y''}{}^{13}+J_{y''y''}{}^{14})+2g_{yy}g_{zy}(-K_{y''z''}{}^{11}+L_{y''z''}{}^{12}-K_{y''z''}{}^{13}+L_{y''z''}{}^{14})]}{(4kT+J_{y''y''}{}^{11}+J_{y''y''}{}^{12}+J_{y''y''}{}^{13}+J_{y''y''}{}^{14})(4kT+J_{z''z''}{}^{11}-J_{z''z''}{}^{12}+J_{z''z''}{}^{13}-J_{z''z''}{}^{14})-(K_{y''z''}{}^{11}+L_{y''z''}{}^{12}-K_{y''z''}{}^{13}+L_{y''z''}{}^{14})^2}, \quad (40)$$

$$\chi_z(T>T_N)=\frac{4\beta^2[g_{zz}^2(4kT+J_{y''y''}{}^{11}-J_{y''y''}{}^{12}+J_{y''y''}{}^{13}-J_{y''y''}{}^{14})+g_{yz}(4kT+J_{z''z''}{}^{11}+J_{z''z''}{}^{12}+J_{z''z''}{}^{13}+J_{z''z''}{}^{14})-2g_{yz}g_{zz}(K_{y''z''}{}^{11}+L_{y''z''}{}^{12}+K_{y''z''}{}^{13}+L_{y''z''}{}^{14})]}{(4kT+J_{y''y''}{}^{11}-J_{y''y''}{}^{12}+J_{y''y''}{}^{13}-J_{y''y''}{}^{14})(4kT+J_{z''z''}{}^{11}+J_{z''z''}{}^{12}+J_{z''z''}{}^{13}+J_{z''z''}{}^{14})-(K_{y''z''}{}^{11}+L_{y''z''}{}^{12}+K_{y''z''}{}^{13}+L_{y''z''}{}^{14})^2}. \quad (41)$$

These expressions are worth some comment. First, it is seen that only in the crystal x direction is the Curie-Weiss law strictly obeyed. The susceptibilities in the other two directions, i.e., in the canting plane, can be expressed in terms of a Curie-Weiss law with a temperature-dependent Weiss constant, and a temperature-dependent Curie constant. At higher temperatures Eqs. (40) and (41) reduce to the simple Curie-Weiss law.

IX. CRYSTAL-FIELD CALCULATION

The only information we have at the present time concerning the g values of the cobalt ion in this material is from the neutron-measured moment at 4.2°K, which indicates that the largest principal g value is at least 6.6, and the static susceptibility measurements of Pauthenet[22] in a powder sample, which indicate that one of the g values is much larger than the other two (see Sec. XI). As the far-infrared resonance measurements give the relative intensities of the absorptions, which are strongly dependent on the g values as well as the angles θ and φ_s [see Eqs. (31) and (32)], it was thought that further information might be obtained from an analysis of the g values within the crystal-field approximation.

Lacking any detailed knowledge of the charge distribution and covalency of the ligands, this was done using a simple point-charge model. Further, to make the analysis as simple as possible, only the ground ^4F term was considered, the ^4P term being neglected. A similar analysis has been given previously[23] in connection with CoF_2. One finds that the ^4F term splits in the octahedral field leaving a $^4T_1$ state lowest. After including the spin-orbit coupling, this $^4T_1$ state splits, with a single Kramer's doublet lying ~ 350 cm^{-1} below all other levels. The level structure is shown schematically in Fig. 9. The crystal-field terms of lower symmetry affect the states in this doublet so as to produce anisotropic g values. As all excited states are so high, at reasonably low temperatures the magnetic properties of the crystal are completely determined by the ground doublet.

Carrying through the analysis one finds that the orbital and spin parts of the g values can be expressed as

$$\begin{aligned} g_{x'}{}^L&=1-(\gamma+\delta), & g_{x'}{}^S&=\tfrac{10}{3}-\tfrac{4}{3}(\gamma+\delta),\\ g_{y'}{}^L&=1+2\gamma, & g_{y'}{}^S&=\tfrac{10}{3}+\tfrac{8}{3}\gamma,\\ g_{z'}{}^L&=1-(\gamma-\delta), & g_{z'}{}^S&=\tfrac{10}{3}-\tfrac{4}{3}(\gamma-\delta), \end{aligned} \quad (42)$$

where δ and γ are parameters determined from the crystal field and radial wave function parameters. It is evident from (42) that whatever their values, the sum of the three g values will be 13, a point useful in analyzing the data. The radial wave functions may be taken to be those of Watson[24] for neutral cobalt, since

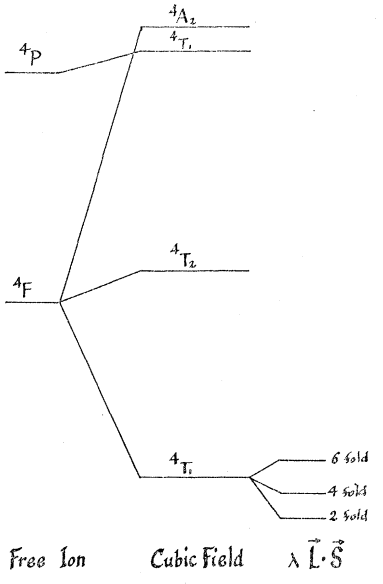

FIG. 9. The electronic splittings of Co^{++} in cubic field and under spin-orbit coupling.

[22] See first footnote in E. F. Bertaut, J. Coing-Boyat, and A. Delapalme, Phys. Letters **3**, 178 (1963); and (private communication).

[23] M. Tinkham, Proc. Roy. Soc. (London) **A236**, 549 (1956).

[24] R. E. Watson, Phys. Rev. **119**, 1934 (1960).

he has shown that the $3d$ wave function is insensitive to the presence or absence of the $4s$ electrons. Using his functions, we find $\langle r^2\rangle=0.358$ Å^2 and $\langle r^4\rangle=0.300$ Å^4. The positions of the point charges forming the distorted octahedron which represents the environment of the cobalt ion may be estimated from the room-temperature structure determination of Rentzeperis.[10] If we attribute a single negative charge to each oxygen atom, a numerical calculation leads to the results

$$\begin{aligned} g_{x'}&=3.82,\\ g_{y'}&=4.69,\\ g_{z'}&=4.49. \end{aligned} \tag{43}$$

These values support the position that $g_{y'}$ is the largest of the principal g values, but evidently the *large* anisotropy required by, e.g., the neutron-measured moment, is not accounted for. Presumably a much more careful treatment of the environment is required.

X. THE EXPERIMENTAL SITUATION

Transmission measurements have been made on powder samples of α-$CoSO_4$ at far-infrared wavelengths and at temperatures from 1.6°K to above the Néel temperature. The samples were prepared by heating reagent grade $CoSO_4\cdot 7H_2O$ to 300°C for 24 h in an atmosphere of argon and identified as α-$CoSO_4$ by x-ray analyses of the powder. The pale violet colored powder was then mixed with a small amount of paraffin wax which served as an adhesive. This was pressed into disks one to 2 (mm) thick and $\frac{1}{2}$ in. in diameter and mounted in the cryostat. The monochromator, bolometer detector, and the far-infrared techniques used have been described elsewhere.[25] The transmission spectrum observed below the Néel temperature was normalized to that taken above T_N. This effectively eliminates all nonmagnetic effects such as lattice absorptions, reflections, etc., which usually are relatively temperature-independent at these low temperatures. The sample temperature was controlled with a resistance heater mounted nearby and monitored with a $\frac{1}{10}$ W, 100-Ω carbon resistor thermometer glued onto the edge of the sample with GE-7031 varnish.

The study of α-$CoSO_4$ resulted in the discovery of three magnetic absorption lines which are shown in Fig. 10 and whose frequencies, relative intensities, and linewidths are given in Table V. (The linewidth is taken to be the interval between the frequencies at which the absorption coefficient is half its maximum value.) The two lines at 20.6 and 25.4 cm^{-1} are similar in width and intensity whereas the highest lying line at 35.8 cm^{-1} is broader and shallower. The linewidths and intensities of the lines are highly temperature-dependent and the lines broaden into each other so that

TABLE V. Antiferromagnetic resonance experimental results ($T\ll T_N$).

	Frequency (cm^{-1})	Linewidth (cm^{-1})	Relative intensities
ω_i	20.6±0.2	1.5	1
ω_j	25.4±0.2	1.5	1
ω_k	35.8±0.6	3.4	0.1

they cannot be resolved from one another at temperatures close to the Néel point. In Table V the relative intensities refer to the ratios of the integrated rf susceptibilities $\int\chi_i''(\omega)d\omega$ of the three lines. The three frequencies are referred to as ω_i, ω_j, and ω_k since they have not been identified with the theoretical expressions (23).

The temperature dependence of the resonance frequencies is shown in Fig. 11. As the temperature is raised, all of the resonance frequencies fall, but much more slowly than the appropriate Brillouin function. The extreme broadening of the lines makes it impossible to follow them any farther than is shown in the diagram. From a naive point of view, one might expect the temperature dependence of the resonance frequencies to be proportional to that of the aligned component of the fictitious spin since by Eq. (23) the square of these frequencies depends on the product of two effective exchange fields, each being proportional to $\langle s\rangle_{\rm av}$. The Brillouin function $B_{1/2}$ is plotted for one of the resonance frequencies in Fig. 11. The discrepancy from the Brillouin function might possibly be accounted for by the theory of Bean and Rodbell[26] for a magnetoelastic effect in ordered magnetic crystals. The exchange interactions which are responsible for the ordering depend upon the interatomic spacing. Since the lattice is deformable, it will distort to increase the exchange coupling and hence lower the free energy due to the exchange interaction, the amount of distortion being

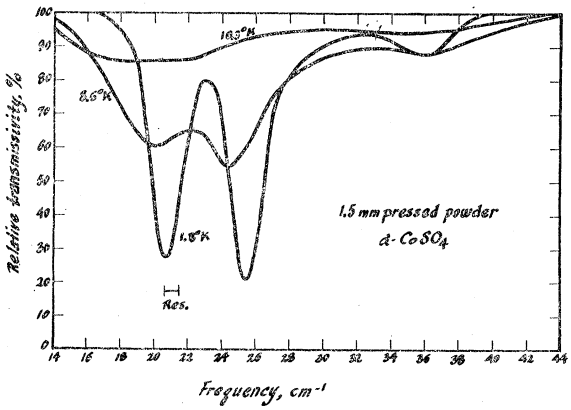

FIG. 10. The far-infrared transmission spectrum at three temperatures.

[25] R. C. Ohlmann and M. Tinkham, Phys. Rev. **123**, 425 (1961); A. J. Sievers, III, and M. Tinkham, *ibid.* **134**, 321 (1961).

[26] C. P. Bean and D. S. Rodbell, Phys. Rev. **126**, 104 (1962).

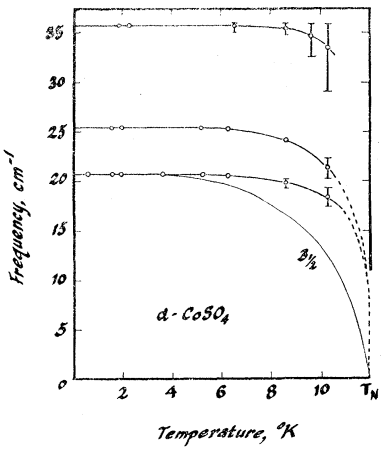

FIG. 11. Temperature dependence of the antiferromagnetic resonance lines and the Brillouin function for $s=\frac{1}{2}$ as a comparison.

limited by the associated increase in free energy due to the lattice strain. At lower temperatures where the spins are more ordered, the exchange energy is greater, causing greater distortion and an increased exchange coupling constant, corresponding to a higher Néel temperature. This "feedback" results in the magnetization maintaining its low-temperature value until the temperature approaches the vicinity of the actual transition point, whereupon the magnetization falls rapidly to zero.[26] In α-$CoSO_4$ the spin system is in close contact with the lattice because of the strong spin-orbit interaction and the large amount of unquenched orbital angular momentum. Consequently, one would expect and unusually strong dependence of exchange coupling parameters on lattice distortion. In addition to the distortion effects, similar behavior of the temperature dependence of the spins follows if biquadratic exchange terms should be included in the Hamiltonian of the system.[27] Moreover, Harris[28] has shown by a Monte Carlo calculation that anomalous magnetization curves can result even with quadratic exchange and a rigid lattice in a case like MnO where there is more than a single important exchange coupling. This result may well have implications for the present case.

Finally, we shall briefly consider the temperature dependence of the sublattice magnetization or spin from the point of view of spin waves.[29] In α-$CoSO_4$ the anisotropy is large and consequently the energy necessary to excite a spin wave is large ($\sim$20–40 cm^{-1}) and the dispersion is small, i.e., the excitation energy at $k=0$ is not too different from that at the zone boundary. Because the Néel temperature, $kT_N\sim 8$ cm^{-1}, is less than half this excitation energy, very few spin waves are thermally excited until the temperature approaches T_N. In this temperature region spin waves should be excited throughout k space, rapidly reducing the sublattice spin. Thus, any of the effects discussed above, or indeed a combination of all of them, might explain the anomalous temperature dependence of the resonance frequencies.

The Néel temperature has been found to be $\sim$12°K by observing the temperature at which the antiferromagnetic line strengths go to zero; this is in agreement with Pauthenet's[22] value which was determined by susceptibility measurements. The powder susceptibility (χ_p) measurements of Pauthenet indicate classical antiferromagnetic behavior, that is

$$\chi_p(0)=\tfrac{2}{3}\chi_p(T_N). \tag{44}$$

This is the behavior one expects of a canted antiferromagnet which can be broken up into pairs of antiparallel sublattices.

In addition, Pauthenet has found the molar powder Curie constant, $C_P=3.12$, and the paramagnetic Curie temperature, $\theta_P=-42$°K. These constants are defined by the high-temperature behavior of the powder susceptibility curve. At lower temperatures ($\sim$80°K down to T_N) a plot of $1/\chi_p$ versus T shows that $1/\chi_p$ decreases with temperature faster than the high-temperature straight-line extrapolation, in qualitative agreement with the behavior expected from our expressions (40) and (41).

Neutron diffraction experiments have furnished useful data: the magnetic structure (Fig. 1), the angle of cant (25°), and the magnetic moment at $T=4.2$°K (3.3 ± 0.2 Bohr magnetons). If φ_m is the angle between the magnetic moment and the single-primed y axis (a principal axis of the g tensor), then $\theta+\varphi_m=25°$. The g value in the equilibrium low-temperature configuration (experimentally 6.6 ± 0.4) is given by Eq. (12). Equations (11) and (13) are also applicable. From Eq. (13) we see that

$$g_{y'}\geq 6.6. \tag{45}$$

XI. THE FITTING PROCEDURE

Within the limits of the present model, the problem could be considered as solved if it were possible to obtain numerical values for the parameters of the Hamiltonian (18). A unique solution is impossible for several reasons: first, the lack of important experimental data, and second, the lack of a reliable theory which might enable us confidently to relate the Néel temperature and the high-temperature susceptibilities with the exchange parameters. In view of the complexity of (18), a useful approach is to make as many approximations as seem physically reasonable, and then see if it is at all possible to reconcile different experimental results using these simplified expressions.

Consideration of Table III and Fig. 4 indicates that the Co_1-Co_3 and the Co_1-Co_4 exchange parameters are likely to be very nearly equal. [This is actually true of the exchange parameters expressed in the crystal coordinates, and is only approximately true in (18)

[27] D. S. Rodbell, I. S. Jacobs, J. Owen, and E. A. Harris, Phys. Rev. Letters 11, 10 (1963); 11, 104 (1963).
[28] E. A. Harris, Phys. Rev. Letters 13, 158 (1964).
[29] We would like to thank Dr. A. Narath of the Sandia Corporation for a discussion of this point.

because of the system of axes we have chosen for representing our Hamiltonian.] Initially, at least, the intrasublattice exchange might be neglected as there is good reason for thinking that these terms are at least a factor of 2 smaller than any other terms in the Hamiltonian (Table III). We are now left with an eight parameter Hamiltonian.

Using Eq. (38) and the experimental value of the Néel temperature we obtain

$$J_0=4kT_N=33.4\ \text{cm}^{-1}. \tag{46}$$

Because of the unavailability of single crystals of α-$CoSO_4$, an unequivocal identification of the observed lines with the frequencies (23) is impossible. (Studies using single crystals and polarized infrared radiation would provide this information.) If we tentatively assign ω_i, ω_j, ω_k, (Table V) to ω_1, ω_3, and ω_5 [Eq. (23)], respectively, then using (46) one obtains:

$$\begin{aligned}4\omega_1^2\hbar^2/(hc)^2&=1697\,(\text{cm}^{-1})^2\\&=(33.4+J_{x''x''}{}^{12}+2J_{x''x''}{}^{13})\\&\quad\times(33.4+J_{z''z''}{}^{12}-2J_{z''z''}{}^{13}),\end{aligned} \tag{47a}$$

$$\begin{aligned}4\omega_3^2\hbar^2/(hc)^2&=2580\,(\text{cm}^{-1})^2\\&=(33.4+J_{x''x''}{}^{12}-2J_{x''x''}{}^{13})\\&\quad\times(33.4+J_{z''z''}{}^{12}+2J_{z''z''}{}^{13}),\end{aligned} \tag{47b}$$

$$\begin{aligned}4\omega_5^2\hbar^2/(hc)^2&=4956\,(\text{cm}^{-1})^2\\&=(33.4-J_{x''x''}{}^{12})(33.4-J_{z''z''}{}^{12}).\end{aligned} \tag{47c}$$

All the interactions between the cobalt ions are assumed to be antiferromagnetic except for that between Co_1 and Co_2 which is taken to be ferromagnetic. Thus, in the Hamiltonian (18) all the parameters are positive with the exception of J^{12} which is negative. As the most direct exchange paths between Co_1 and Co_2 are much shorter and less complicated than any of the others, J^{12} is expected to be the largest set of exchange parameters, perhaps by an order of magnitude, although a look at the basic interactions shows that J^{12} can have both ferromagnetic and antiferromagnetic components, the sum of which could reduce its absolute magnitude. This choice of interactions also gives the spin configuration associated with the root given in Eq. (38) the highest degree of stability since the Néel temperature is then maximized. Taking cognizance of the remarks above, we can easily see the difficulty of reconciling the Néel temperature with the far-infrared results (47) (if the molecular field calculation is assumed to be valid). The situation would be somewhat improved if the intrasublattice interaction were large and antiferromagnetic; however, this does not seem too reasonable. Again, if we assume that distortions are taking place at low temperatures, then the exchange would have a temperature dependence such as to increase the effective value of T_N which the system "feels" at temperatures much lower than the transition temperature. If this is the case, then it is not valid to use the value of T_N given in (46), but a larger value which would indeed aid in the fitting of Eqs. (47). In order to use Eqs. (32) for the line intensities in the fitting procedure, we require more accurate knowledge of the g values and the angle θ.

We can get information about the g values from measurements of the powder susceptibility

$$\chi_P=C_P/(T-\theta_P)+\chi_\infty. \tag{48}$$

Above 80°K, Pauthenet was able to fit his data with $C_P=3.12$, $\theta_P=-42$°K, and $\chi_\infty=0$. We have replotted Pauthenet's data on a plot of $\chi_P T$ versus T rather than $1/\chi_P$ versus T:

$$\chi_P T=C_P/(1-\theta_P/T)+\chi_\infty T. \tag{49}$$

This method brings out the temperature-independent term as the slope of the high-temperature straight-line fit, with the intercept of the χT axis giving C_P. It is difficult to extract an accurate value of θ_P for α-$CoSO_4$ in this type of plot because at high temperatures it is suppressed, and at low temperatures, the susceptibility deviates from the Curie-Weiss law due to either the approach of the Néel temperature [see Eqs. (40) and (41)], or due to the depopulation of a low-lying excited doublet. We have not observed the latter. We find $C_P=2.3$, $\chi_\infty=0.15\times10^{-2}$, and θ_P between -10 and -15°K.

If we take the proper average for a powder sample, we find

$$C_P=N_0\beta^2\langle g^2\rangle_{\text{av}}/4k, \tag{50}$$

where N_0 is Avogadro's number,

$$\langle g^2\rangle_{\text{av}}=\tfrac{1}{3}(g_{x'}{}^2+g_{y'}{}^2+g_{z'}{}^2),$$

and k is the Boltzmann constant. Solving gives $(g_{x'}{}^2+g_{y'}{}^2+g_{z'}{}^2)\approx74$, taking $C_P=2.3$. This, together with the constraint

$$g_{x'}+g_{y'}+g_{z'}=13, \tag{51}$$

which follows from the crystal-field theory [see Eq. (42)] and is known to be obeyed by many cobalt salts for which paramagnetic resonance data exist, informs us that one of the g values, i.e., $g_{y'}$ must be much larger than the other two. From Eqs. (50) and (51), it is seen that $g_{y'}$ must be between 7 and 8 which is in agreement with the neutron diffraction data. These deductions are only valid if the nearest excited doublet is sufficiently high so as not to contribute to the susceptibility in the temperature region where Pauthenet's data were fitted.

It must unfortunately be concluded that it is impossible to deduce meaningful values for the parameters in this problem with the present limited experimental data. It is hoped that the growth of single crystals in the near future will enable further progress to be made. The availability of single crystals would permit the definite identification of the modes; static susceptibility measurements will yield the three χ's at $T=0$

[Eqs. (33)], the three χ's at $T=T_N$, the three high-temperature Curie constants C, and the three Weiss constants θ_P [Eqs. (39)–(41)]. These data would transform the situation and make possible a meaningful fit.

XII. CONCLUSION

By analyzing the magnetic properties of α-$CoSO_4$ it has become apparent that an exchange interaction isotropic in the true spin is quite inadequate to describe this problem. The fact that in an octahedral environment, cobalt has a degenerate orbital triplet results in its orbital angular momentum remaining largely unquenched by the crystalline field. Octahedral distortions can give rise to large anisotropic exchange interactions, the source of the anisotropy being the spin-orbit interaction. By considering the system in terms of the fictitious spin of $\frac{1}{2}$, we have seen that the anisotropic g tensor can give rise to additional effective anisotropic and antisymmetric exchange. Use of the isotropic fictitious spin enables one to analyze easily the dynamical and static properties of the crystal, as compared to the difficulties that would be encountered if one attempted to approach the problem in terms of the true spins or magnetic moments. In addition, our method of writing down the Hamiltonian and using a system of nonorthogonal axes seems to be a useful technique for this and other problems. This same approach is used to treat the four-sublattice noncoplanar canted antiferromagnetic β-$CoSO_4$ in work now in preparation.

Experimentally the far-infrared studies have yielded valuable information about α-$CoSO_4$ and a far-infrared mode whose existence is due to the spins being canted has been observed.

The impossibility of reconciling the Néel temperature and the resonance frequencies using a molecular field model is apparent. As was explained in the last section, some sort of progressive distortion and a temperature-dependent T_N could possibly be responsible, and x-ray determinations of the crystal structure at helium temperatures would be of great interest. An additional explanation is the inadequacy of the molecular field method. Even in simple cases this approximation is known to be inadequate. A proper treatment of the α-$CoSO_4$ system allowing for the effects of long- and short-range order and anisotropy might aid in removing these discrepancies, and also give the observed temperature variation of the resonance frequencies.

ACKNOWLEDGMENTS

We would like to thank Dr. R. Pauthenet for providing us with unpublished static susceptibility data. One of us (J.H.M.T.) is indebted to the Commonwealth Fund for a Harkness Fellowship.

APPENDIX

We would like to find the temperature dependence of $\mathbf{s}$ with the Hamiltonian

$$\mathcal{H}=c_x s_x+c_y s_y+c_z s_z.$$

Using the Pauli spin-$\frac{1}{2}$ matrices, we diagonalize the Hamiltonian to find energy eigenvalues:

$$\epsilon_i=\pm\tfrac{1}{2}(c_x^2+c_y^2+c_z^2)^{1/2}=\pm\epsilon,$$

with corresponding eigenfunctions

$$|a\rangle=\cos\varphi|+\rangle+\sin\varphi e^{i\psi}|-\rangle,$$
$$|b\rangle=-\sin\varphi|+\rangle+\cos\varphi e^{i\psi}|-\rangle,$$

where

$$\tan 2\varphi=(c_x^2+c_y^2)^{1/2}/c_z,$$
$$\tan\psi=c_y/c_x.$$

We then evaluate

$$\langle s_i\rangle_T=\sum_{j=a,b}\langle j|s_i|j\rangle e^{-\epsilon_j/kT}/\sum_{j=a,b}e^{-\epsilon_j/kT}$$

to find

$$\langle s_z\rangle_T=-\tfrac{1}{2}\cos 2\varphi\tanh(\epsilon/kT),$$
$$\langle s_x\rangle_T=-\tfrac{1}{2}\sin 2\varphi\cos\psi\tanh(\epsilon/kT),$$
$$\langle s_y\rangle_T=-\tfrac{1}{2}\sin 2\varphi\sin\psi\tanh(\epsilon/kT).$$

In the limit $\epsilon/kT\ll 1$, these all reduce to

$$\langle s_i\rangle_T=-c_i/4kT,\quad i=x,y,z.$$